Electronic Supplementary Information

Multi-stacked hyperporous silicon flake for highly active solar hydrogen production

Youn Jeong Jang[a,†], Jaegeon Ryu[b,†], Dongki Hong[b], Soojin Park[b,*] and Jae Sung Lee[b,*]

[a] Department of Chemical Engineering, Pohang University of Science and Technology (POSTECH), Pohang 790-784, South Korea

[b] Department of Energy Engineering, School of Energy and Chemical Engineering, Ulsan National Institute of Science and Technology (UNIST), Ulsan 44919, South Korea

[*]Corresponding Authors:

Soojin Park, spark@unist.ac.kr

Jae Sung Lee, jlee1234@unist.ac.kr

[†] These authors contributed equally to this work.

Experimental details

Synthesis of MHSF

Talc (CP grade), micro-sized magnesium powders, hydrochloric acid (35.0-37.0%, HCl, EP grade), and sodium chloride (99.5%, GR grade) were supplied by Samchun Chemical Co., Ltd, South Korea. All chemicals were used as received without any further purification. The MHSF was prepared by magnesiothermic reduction and subsequent simple acid leaching process. Firstly, commercially available Talc clay was uniformly mixed with magnesium powder in a weight ratio of 1:0.6 (with theoretical calculation for fully reduction of silicon dioxide components). The mixture was transferred to a stainless steel reactor in an argon (Ar) atmosphere. Then this reactor was placed in a tube furnace and heated to high temperature (650 ^{o}C) for 3 h. After completion of reaction, the resulting powder was dissolved in 100 mL of deionized water under mild stirring for 3 h to untangle the particles. Subsequently, 1 M HCl was added to this solution, and additionally stirred at room temperature for 3 h to eliminate MgO by-products. As-prepared MHSF were directly used as an anode material for LIBs. Meanwhile, for photocatalytic measurement, it was further leached out native oxide layers with 0.5% HF solution for 10 min. The production yield of as-synthesized MHSF reaches about 25% which is very close to theoretical value (~28%). Until photocatalytic measurement, it should be avoided for moisture.

Physical characterization

SEM (Verios 460, FEI) was used to characterize the surface morphologies of MHSF samples at an acceleration voltage of 10 kV and current of 0.4 nA. The dimensions and internal

structures of MHSF were determined using TEM (JEOL-2100) and HRTEM (JEOL-2100C) at an acceleration voltage 200 kV. To investigate the microstructures and degrees of crystallinity of MHSF samples, XRD analyses (D8 ADVANCE, Bruker) were performed using Cu-Kα radiation (λ = 1.5418 Å); Raman spectroscopy (alpha300R confocal microscope, WlTec) was also employed for this purpose. The pore sizes and surface areas were characterized using surface area and pore size analyser (BELSORP-mini II, BEL Japan, Inc.) at 77 K for P/P_0 of 0.05–0.3. XPS (Thermo Fishers K-alpha, UK) was used to perform surface elemental analyses. Further, the elemental components were confirmed using inductively coupled plasma-mass spectrometry (ELAN DRC-II).

Optical properties and band alignments

The optical band gap energy of MHSF can be estimated from its Tauc plot using the following relationship: $\alpha\, h\upsilon = A\,(h\upsilon - E_g)^{n/2}$, where α, $h\upsilon$, A, E_g, and n are the absorption coefficient, the photon energy, a constant, the optical band gap energy, and the transition constant, which depend on the band gap properties (i.e., direct (n = 1) or indirect (n = 4)). The band gap was calculated by extrapolating the linear part of the $(\alpha h\upsilon)^2$ vs. $h\upsilon$ plot to the x-axis. The optical properties of MHSF were measured using a UV-Vis diffuse reflectance spectrometer (UV-2401PC, Shimadzu Corp.) equipped with integrating spheres. The optical reflectance was recorded at room temperature for wavelengths of 200–1000 nm and $BaSO_4$ was used as the reference. The position of the Si valence band was determined by UPS (ESCALAB 250Xi, monochromated Al-Kα radiation) under a base pressure of 10^{-10} Torr.

Photocatalytic hydrogen evolution

The light-induced activities of Si photocatalysts with respect to reduction of water were measured on the basis of the amount of H_2 gas generated from an Ar-saturated aqueous solution containing methanol (10 vol%, 100 mL) as a hole scavenger. The water/methanol mixture was purged with Ar for 2 h, and 0.1 g of the Si photocatalyst being tested was added to it in a closed Pyrex glass vessel (~193.5 mL). The photocatalytic water-reduction reaction was performed under ambient conditions using a Xe lamp (300 W, Oriel) equipped with an optical UV cut-off filter ($\lambda \geq 400$ nm) as a light source, with the mixture being subjected to mild stirring. Using Ar as the carrier gas, the amount of H_2 gas evolved was measured with a gas chromatography (GC) system equipped with a thermal conductivity detector (HP 7890, molecular sieve 5 Å column). To evaluate the stability of the catalysts, the photocatalytic hydrogen evolution tests were performed for 3 cycles of 6 h each; these were separated by a 2-h-long reaction under dark conditions Ar purging to remove the hydrogen produced in the previous cycle. The amount of hydrogen produced from stoichiometric etching of Si using KOH as a function of time was also measured using GC. All the chemical reactions were performed in a 193.5 mL glass flask with a tightly fitted rubber septum. The hydrogen production tests were repeated at least 10 times using a 1 M aqueous KOH solution.

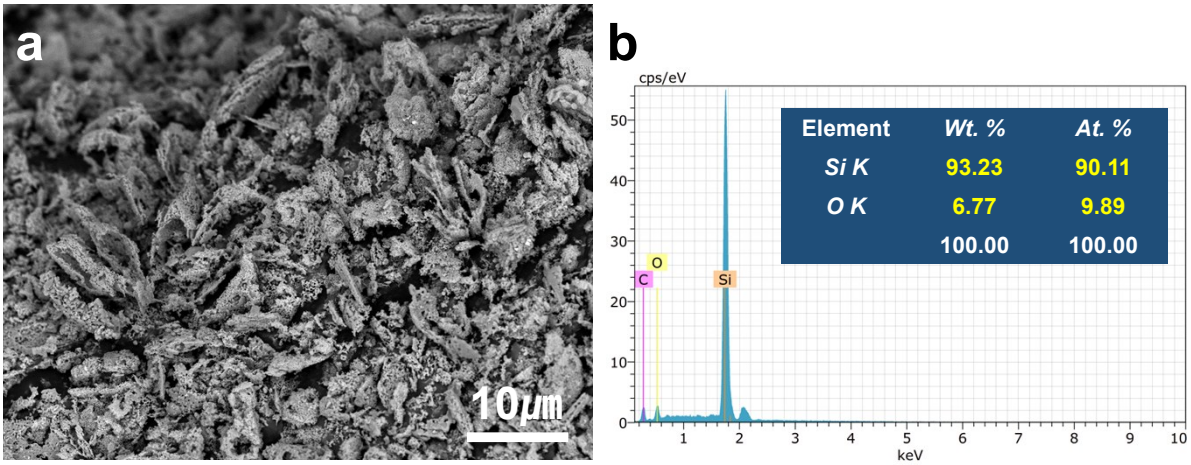

Figure S1. (a) SEM image and (b) EDX spectrum of MHSF

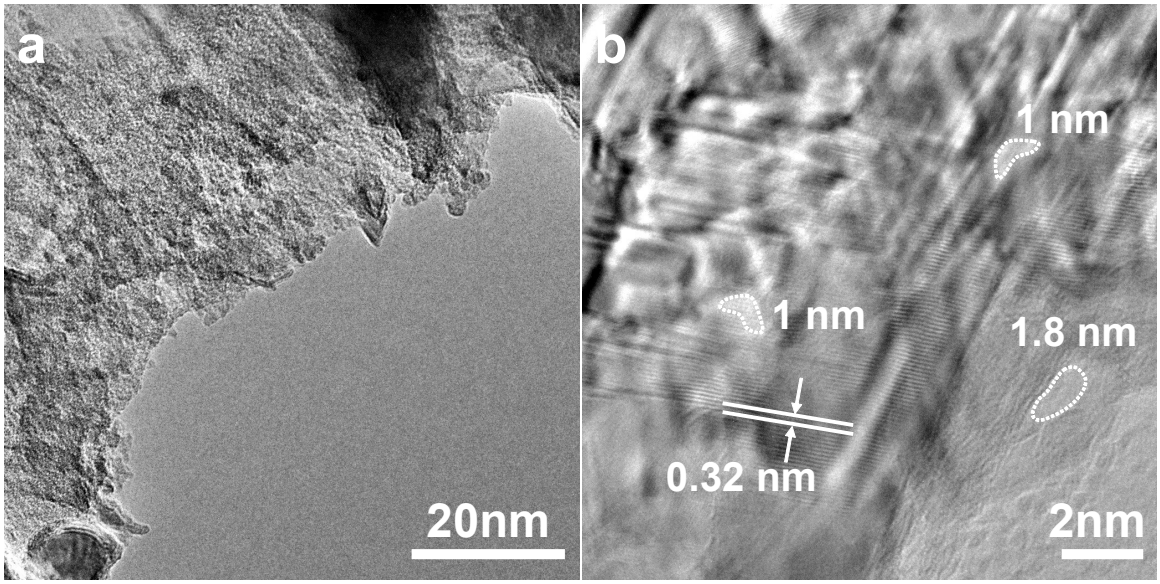

Figure S2. Analysis for surface nanopores on MHSF. (a-b) TEM images showing nanopores less than 2nm over the MHSF framework.

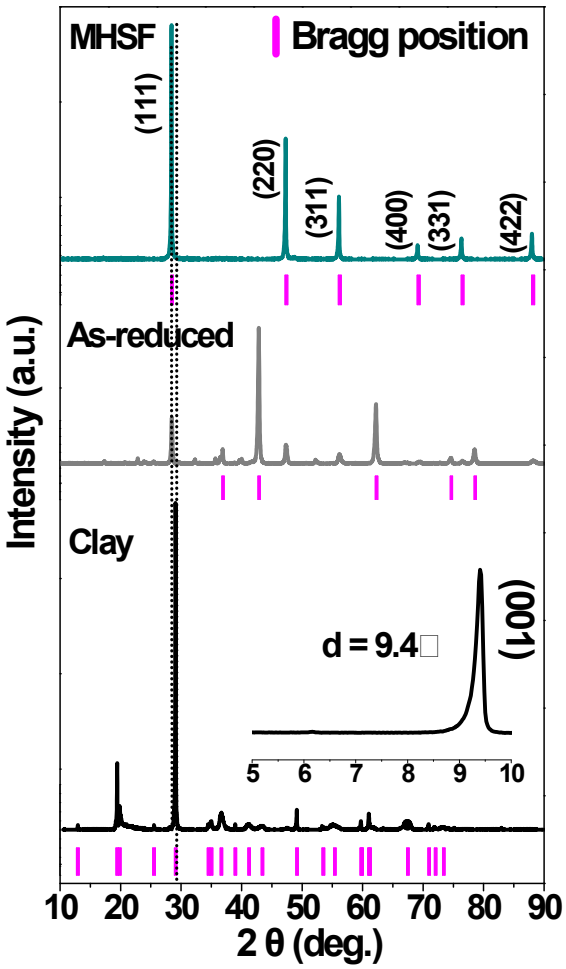

Figure S3. X-ray diffraction (XRD) pattern of MHSF. Phase transition from bare clay minerals (bottom) to intermediate state (middle) and finally pure silicon state (top). (inset. High-power XRD pattern of bare clay minerals)

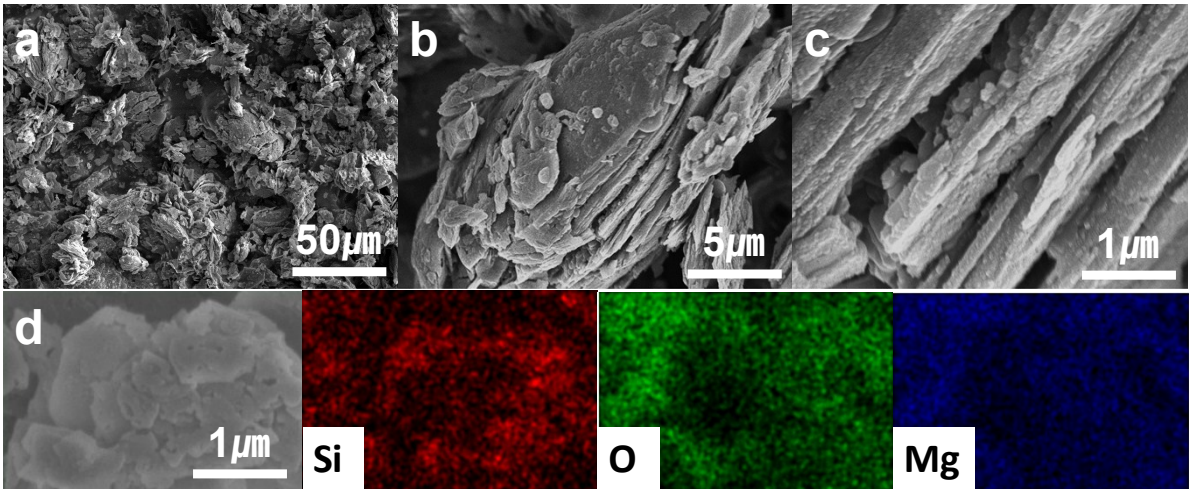

Figure S4. Analysis for as-reduced MHSF. (a-c) SEM images, (d) EDX elemental maps data.

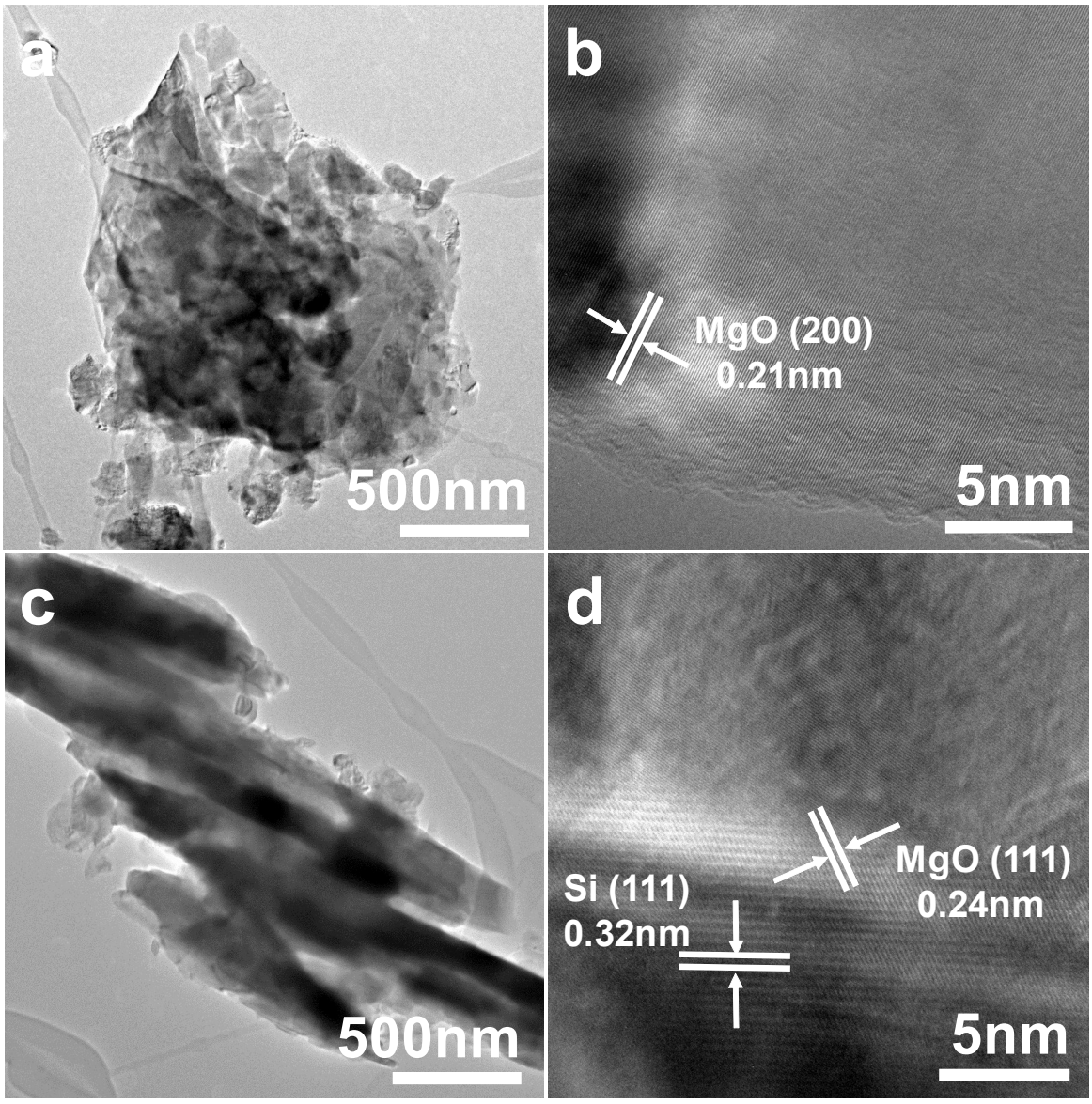

Figure S5. Analysis for as-reduced MHSF. TEM (a-b) top surface and (c-d) side surface images of intermediate state of MHSF.

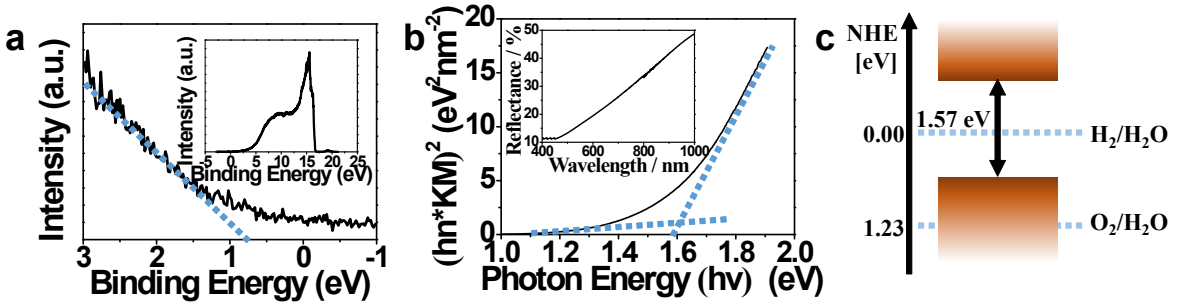

Figure S6. Optical properties of MHSF. (a) UPS spectra, (b) Tauc plots (inset: UV-Vis diffuse reflectance spectra) and (c) Band alignment of MHSF.

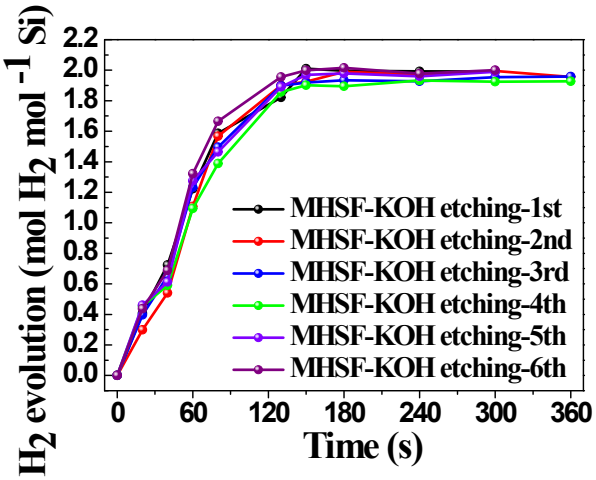

Figure S7. Hydrogen generation measurements of MHSF for KOH chemical etching reaction.

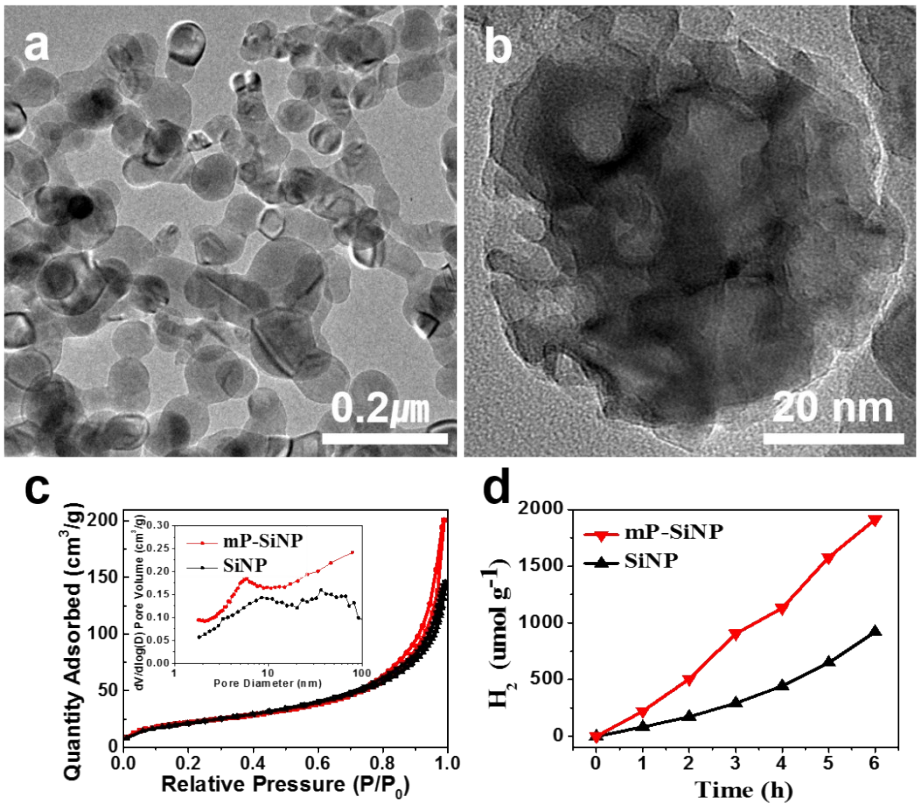

Figure S8. Analysis and photocatalytic performance of SiNP and mP-SiNP. TEM images of (a) SiNP and (b) mP-SiNP. (c) Nitrogen adsorption-desorption isotherm curve (inset. BJH pore size distribution curve). (d) Amounts of hydrogen generated using SiNP and mP-SiNP under visible-light.

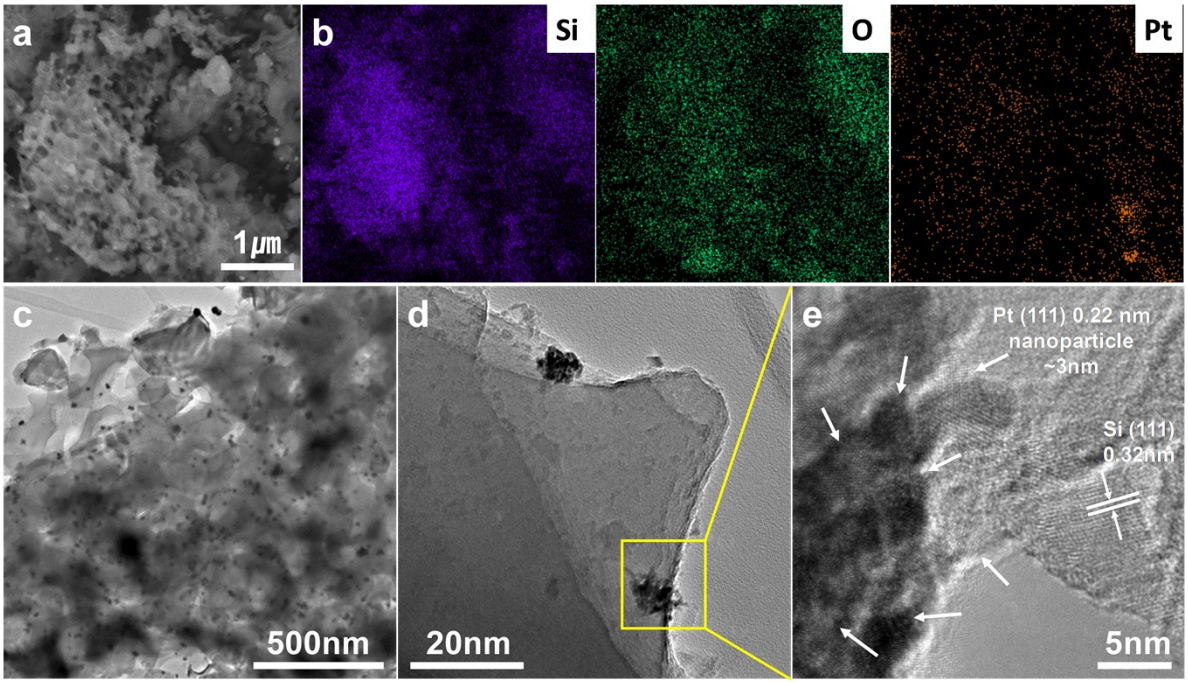

Figure S9. Characterization of MHSF @Pt. (a) SEM image, (b) EDX elemental maps and (c-e) TEM images.

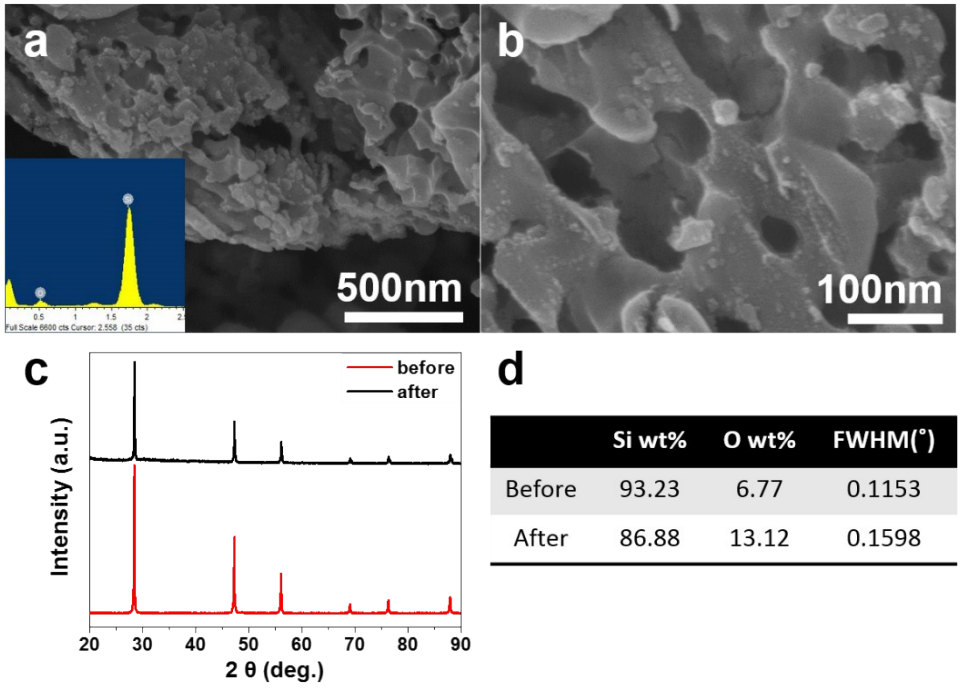

	Si wt%	O wt%	FWHM(°)
Before	93.23	6.77	0.1153
After	86.88	13.12	0.1598

Figure S10. Characterization of after-reacted MHSF (a-b) SEM image (inset. EDX spectrum), (c) XRD pattern and (d) summary chart for EDX quantification and FWHM values.

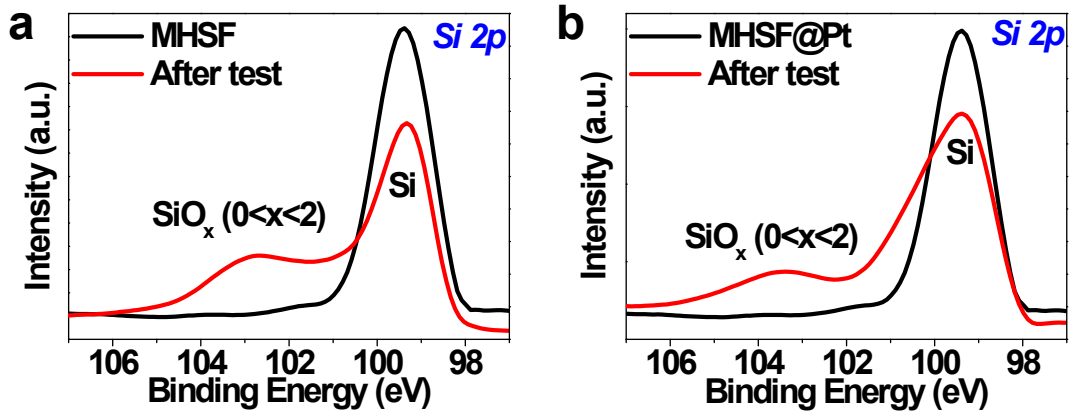

Figure S11. Si 2p XPS spectra of (a) MHSF and (b) MHSF@Pt before/after long-term photocatalytic test.

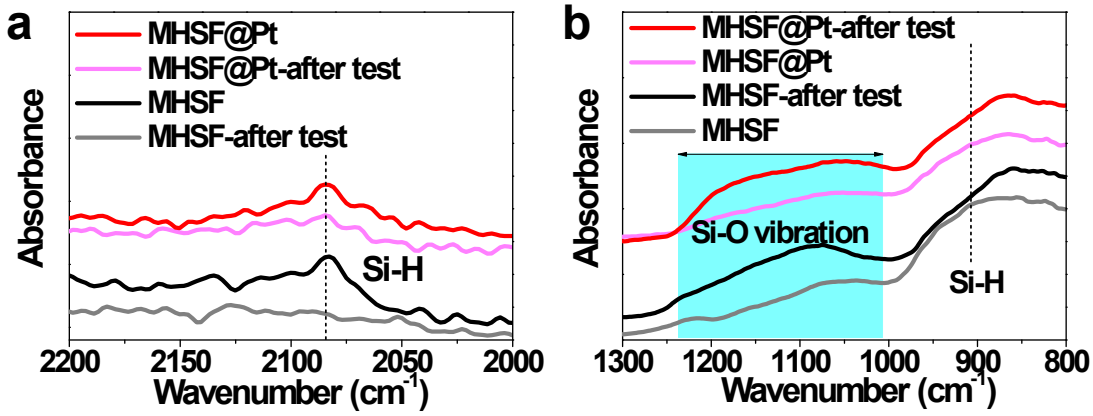

Figure S12. FT-IR spectra of as-prepared and tested MHSF and MHSF@Pt at (a) 2200-2000 cm^{-1} and (b) 1300-800 cm^{-1}.

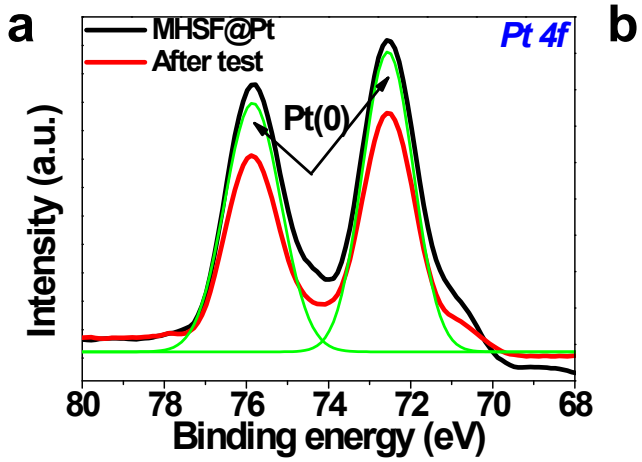

b

Element		Wt. %	At. %
Si K	*Before*	87.88	82.20
	After	72.34	67.11
O K	*Before*	9.07	17.41
	After	25.55	32.64
Pt M	*Before*	3.05	0.39
	After	2.11	0.25

Figure S13. (a) Pt 4f XPS spectra and (b) Composition table of MHSF@Pt before/after long-term photocatalytic test.

Table S1. Summary of photocatalytic hydrogen production activity of Si-based materials and various semiconductor photocatalysts.

Photocatalyst	Structure	Eg (eV)	Light source	Incident light	Aqueous reaction solution	Activity ($\mu mol\ h^{-1} g^{-1}$) Co-cat / H^2	Ref.
MHSF	**Nanoflake**	**1.57**	**300W -Xe**	**λ > 400nm**	**Water/methanol (10 vol. %)**	**709**	**This work**
MHSF@Pt	**Nanoflake**					**1031**	
Mesoporous Si nanoparticle	Nanoparticle	1.62	300W -Xe	λ > 400nm	Water/methanol (15 vol. %)	~640	13
Si nanoparticle	Nanoparticle	1.8	300W -Xe	λ > 400nm	Water/methanol (10 vol. %)	153	14
Mesoporous Si nanoparticle						356	
Si nanosheet	Nanosheet	1.9				486	
						Pt / 723	
$g\text{-}C_3N_4$	Nanoplatelet	2.7	300W -Xe	λ > 420nm	Water/methanol (10 vol. %)	Pt / ~100	1*
CDot- C_3N_4	Nanoplatelet	2.77	300W -Xe	λ > 420nm	Ultrapure water	105	2*
Graphene / $g\text{-}C_3N_4$	Nanosheet	2.7	350W -Xe	λ > 400nm	Water/methanol (25 vol. %)	Pt / ~1500	3*
MoS_2 / $g\text{-}C_3N_4$	Nanosheet	2.7	300W -Xe	λ > 400nm	Water/methanol (25 vol. %)	Pt / ~230	4*
Zn-In-S	Nanolayer	2.32	400W -Hg	λ > 420nm	Water / triethanolamine	Pt / ~1000	5*
CdSe	Nanoribbon	2.7	300W -Xe	λ > 450nm	0.1M Na_2S / 0.1M Na_2SO_3	MoS_2 / 900	6*
CdS	Nanosheet	2.25	300W -Xe	λ > 420nm	0.35M Na_2S / 0.23M Na_2SO_3	Pt / ~24,000	7*

Graphene-CdS	Nanosheet	2.25	350W -Xe	λ > 420nm	Water / lactic acid (10 vol. %)	Pt / ~56,000	8*
CuS-ZnS	Nanosheet	3.35	350W -Xe	λ > 420nm	0.35M Na_2S / 0.23M Na_2SO_3	4,147	9*
TiO_2	Nanosheet	3.25	150W -Xe	UV	Water/methanol (50 vol. %)	Pt / 6,000	10*
Ni_xO_y/ MCM-48	Nanocluster	3.52	300W -Xe	λ > 280nm	Water/methanol (mol ratio 1:8)	~2750	11*
Ni / g-C_3N_4	Nanoribbon	2.75	300W -Xe	λ > 400nm	Water/TEOA (30 vol. %)	~4000	12*
$ZnFe_2O_4$/C	Nanosphere	~2.75	300W -Xe	λ > 420nm	Water/methanol (10 vol. %)	1160.40	13*
Ru-doped TiO_2	3D sea urchin	3.09	150W -Xe	625nm> λ >400nm	Water/methanol (20 vol. %)	~100	14*
g-C_3N_4 (Tris-s-triazine)	Nanosheet	1.17	300W -Xe	λ > 420nm	Water/TEOA (10 vol. %)	Pt / 15,000	15*
$Cu_{1.94}S$/ $Zn_{0.23}CdS$	Nanorod	2.83	300W -Xe	λ > 420nm	0.1M Na_2S / 0.1M Na_2SO_3	Pt / 13,533	16*
TiO_2/rGO	Nanosheet	2.10	300W -Xe	λ > 400nm	Water/methanol (20 vol. %)	Pt / 890	17*
CeO_x	Nanodot	~2.6	200W -W	λ > 400nm	Water/Ethanol (5 vol. %)	Pt / 13,533	18*
TiO_2/ZrO_2	Hollow sphere	3.18	300W -Xe	λ > 400nm	Water/Na_2S	~30	19*
Li_xMoS_2/ $Zn_{0.5}Cd_{0.5}S$	Nanosheet	2.58	300W -Xe	λ > 420nm	0.25M Na_2S / 0.25M Na_2SO_3	7,699	20*

***=Supplementary references**

References

1 X. C. Wang, K. Maeda, A. Thomas, K. Takanabe, G. Xin, J. M. Carlsson, K. Domen and M. Antonietti, *Nat. Mater.* 2009, **8**, 76-80.

2 J. Liu, Y. Liu, N. Y. Liu, Y. Z. Han, X. Zhang, H. Huang, Y. Lifshitz, S. T. Lee, J. Zhong and Z. H. Kang, *Science* 2015, **347**, 970-974.

3 Q. J. Xiang, J. G. Yu and M. Jaroniec, *J. Phys. Chem. C* 2011, **115**, 7355-7363.

4 L. Ge, C. C. Han, X. L. Xiao and L. L. Guo, *Int. J. Hydrogen Energy* 2013, **38**, 6960-6969.

5 Z. D. Xu, Y. X. Li, S. Q. Peng, G. X. Lu and S. B. Li, *Rsc Adv.* 2012, **2**, 3458-3466.

6 F. A. Frame and F. E. Osterloh, *J. Phys. Chem. C* 2010, **114**, 10628-10633.

7 N. Z. Bao, L. M. Shen, T. Takata and K. Domen, *Chem. Mater.* 2008, **20**, 110-117.

8 Q. Li, B. D. Guo, J. G. Yu, J. R. Ran, B. H. Zhang, H. J. Yan and J. R. Gong, *J. Am. Chem. Soc.* 2011, **133**, 10878-10884.

9 J. Zhang, J. G. Yu, Y. M. Zhang, Q. Li and J. R. Gong, *Nano Lett.* 2011, **11**, 4774-4779.

10 Y. L. Zhang, T. Xia, M. W. Shang, P. Wallenmeyer, D. Katelyn, A. Peterson, J. Murowchick, L. F. Dong and X. B. Chen, *Rsc Adv.* 2014, **4**, 16146-16152.

11 R. Peng, K. Shrestha, G. Mishra, J. Baltrusaitis, C. –M. Wu and R. T. Koodali, *RSC Adv*. 2016, **6**, 59169-59180.

12 L. Kong, Y. Dong, P. Jiang, G. Wang, H. Zhang and N. Zhao, *J. Mater. Chem. A* 2016, **4**, 9998-10007.

13 H. Zhu, M. Fang, Z. Huang, Y. Liu, K. Chen, C. Tang, M. Wang, L. Zhang and X. Wu, *RSC Adv*. 2016, **6**, 56069-56076.

14 T. –D. Nguyen-Phan, S. Luo, D. Vovchok, J. Llorca, S. Sallis, S. Kattel, W. Xu, L. F. J. Piper, D. E. Polyansky, S. D. Senanayake, D. J. Stacchiola and J. A. Rodriguez, *Phys. Chem. Chem. Phys*. 2016, **18**, 15972-15979.

15 L. Lin, H, Ou, Y. Zhang and X. Wang, *ACS Catal*. 2016, **6**, 3921-3931.

16 Y. Chen, S. Zhao, X. Wang, Q. Peng, R. Lin, Y. Wang, R. Shen, X. Cao, L. Zhang, G. Zhou, J. Li, A. Xia and Y. Li, *J. Am. Chem. Soc*. 2016, **138**, 4286-4289.

17 L. Li, L. Yu, Z. Lin and G. Yang, *ACS Appl. Mater. Interfaces* 2016, **8**, 8536-8545.

18 N. R. Manwar, A. A. Chilkalwar, K. K. Nanda, Y. S. Chaudhary, J. Subrt, S. S.

Rayalu and N. K. Labhsetwar, *ACS Sustainable Chem. Eng*. 2016, **4**, 2323-2332.

19 J. Zhang, L. Li, Z. Xiao, D. Liu, S. Wang, J. Zhang, Y. Hao and W. Zhang, *ACS Sustainable Chem. Eng*. 2016, **4**, 2037-2046.

20 H. Du, H. –L. Guo, Y. –N. Liu, X. Xie, K. Liang, X. Zhou, X. Wang and A. –W. Xu, *ACS Appl. Mater. Interfaces* 2016, **8**, 4023-4030.